Acta Cryst. (1983). A**39**, 601–608

Theory of Multilayer Neutron Monochromators

BY V. F. SEARS

Atomic Energy of Canada Limited, Chalk River, Ontario, Canada K0J 1J0

(*Received* 7 *September* 1982; *accepted* 16 *February* 1983)

Abstract

The theory of the reflecting properties of multilayer monochromators is developed on the basis of both the kinematical and the dynamical theory of neutron scattering with emphasis on the way in which the flux and polarization of the reflected beam depends on the parameters that characterize the multilayer. The effect of random variations in layer thickness is investigated using a cumulant expansion method. The contamination of the reflected beam due to both higher-order Bragg reflections and specular reflection is also discussed.

1. Introduction

A thin-film multilayer consisting of alternating layers of two different materials, usually Ge–Mn or Ge–Fe, is effectively a one-dimensional 'crystal' that can be used to Bragg reflect a monoenergetic neutron beam out of an initial polyenergetic spectrum (Schoenborn, Caspar & Kammerer, 1974). In addition, if one of the materials is ferromagnetic the Bragg-reflected beam will be polarized (Lynn, Kjems, Passell, Saxena & Schoenborn, 1976). These devices are becoming of increasing interest particularly for use in polarized-beam spectrometers.

The present article contains a detailed theoretical treatment of the properties of multilayer neutron monochromators with emphasis on the way in which the flux and polarization of the reflected beam depend on the parameters that characterize the multilayer. Among other things, we take into account the effect of extinction due to multiple Bragg reflection as well as the effect of random variations in layer thickness that are always present in any real monochromator. We also discuss the contamination effects that arise both from higher-order Bragg reflections and from specular reflection.

Our approach differs from that of Saxena & Schoenborn (1975, 1977) in two important respects. Firstly, we base our discussion on the general expression for the coherent elastic scattering cross section instead of using the Fresnel-zone construction that Saxena & Schoenborn have adapted from the X-ray literature. Secondly, unlike Saxena & Schoenborn, we do not confine our attention to the value of the reflectivity at the center of the Bragg peak. The reflected neutron flux, which is the primary quantity of interest in the present application, depends on the integrated reflectivity rather than the peak reflectivity and these two quantities have, as we shall see, quite different dependences on, for example, the number and thickness of the bilayers.

2. Reflected neutron flux

Fig. 1 represents an idealized multilayer monochromator consisting of alternating layers of two different materials A and B that have been deposited by vacuum evaporation or sputtering on a suitable substrate such as an optical flat. A collimated monoenergetic neutron beam with wavelength λ and angle of incidence θ will be Bragg reflected if $\lambda \simeq \lambda_m$, where λ_m is the wavelength for the mth-order reflection,

$$m\lambda_m = 2d \sin \theta. \tag{2.1}$$

Here d is the repeat distance and $m = 1, 2, 3, \ldots$. In addition, neutrons of any wavelength may be specularly reflected.

In practice, the incident beam will be polyenergetic. Let the total incident flux (neutrons cm^{-2} s^{-1}) be denoted by

$$\Phi = \int_0^\infty \Phi(\lambda)\, \mathrm{d}\lambda, \tag{2.2}$$

where $\Phi(\lambda)\, \mathrm{d}\lambda$ is the incident flux in $\mathrm{d}\lambda$. The reflected flux can similarly be expressed as

$$\Phi' = \int_0^\infty \Phi'(\lambda)\, \mathrm{d}\lambda. \tag{2.3}$$

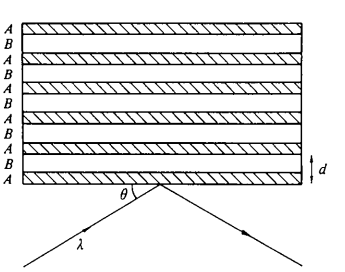

Fig. 1. Multilayer monochromator.

The relation between the incident and reflected flux is determined by the reflectivity of the monochromator, $R(\lambda)$, which is defined as the fraction of incident neutrons with wavelength λ that are reflected when θ has some fixed value. Thus,

$$R(\lambda) = \Phi'(\lambda)/\Phi(\lambda), \tag{2.4}$$

and

$$\Phi' = \int_0^\infty R(\lambda)\Phi(\lambda)\,d\lambda. \tag{2.5}$$

The reflectivity can be expressed as

$$R(\lambda) = R_s(\lambda) + \sum_{m=1}^{\infty} R_m(\lambda), \tag{2.6}$$

where $R_s(\lambda)$ is the contribution from specular reflection and $R_m(\lambda)$ that from the mth-order Bragg reflection. These quantities are illustrated qualitatively in Fig. 2. In particular, $R_s(\lambda)$ begins at small λ being proportional to λ^4 and increases monotonically until it reaches unity at the critical wavelength λ_c. The Bragg peaks are superimposed on top of $R_s(\lambda)$ and have the property that $R_m(\lambda) \simeq 0$ unless $\lambda \simeq \lambda_m$. Hence,

$$\Phi' = \Phi'_s + \sum_{m=1}^{\infty} \Phi'_m, \tag{2.7}$$

where Φ'_s is the contribution from specular reflection,

$$\Phi'_s = \int_0^\infty R_s(\lambda)\Phi(\lambda)\,d\lambda, \tag{2.8}$$

and Φ'_m that from the mth-order Bragg reflection,

$$\Phi'_m = \beta_m\,\Phi(\lambda_m), \tag{2.9}$$

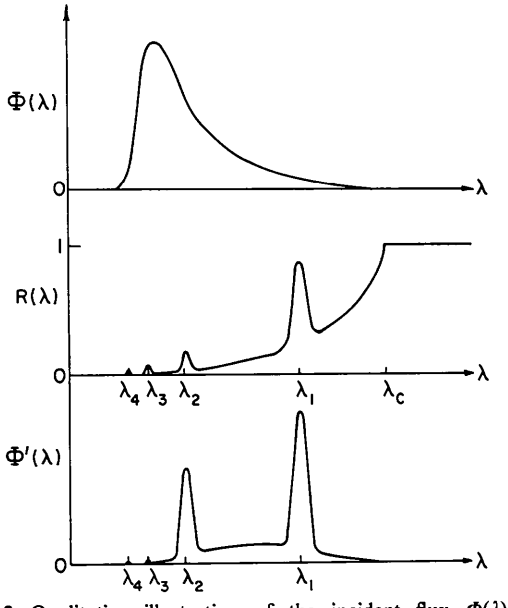

Fig. 2. Qualitative illustration of the incident flux $\Phi(\lambda)$, the reflectivity $R(\lambda)$, and the reflected flux $\Phi'(\lambda)$.

in which β_m is the integrated reflectivity,

$$\beta_m = \int_0^\infty R_m(\lambda)\,d\lambda. \tag{2.10}$$

The features in Fig. 2 have been greatly exaggerated for purposes of clarity. In fact, almost all of the reflected flux will be in the first-order Bragg peak at λ_1; otherwise one would not have a useful monochromator. Thus, it is convenient to write

$$\Phi' = \Phi'_1\left(1 + C_s + \sum_{m=2}^{\infty} C_m\right). \tag{2.11}$$

where C_s represents the contamination due to specular reflection,

$$C_s = \Phi'_s/\Phi'_1, \tag{2.12}$$

and C_m the contamination due to the mth-order Bragg reflection,

$$C_m = \Phi'_m/\Phi'_1. \tag{2.13}$$

The primary purpose of the present work is to provide the theoretical background that will help one to design a multilayer monochromator for which the first-order reflected flux Φ'_1 is as large as possible, while, at the same time, C_s and C_m are kept negligibly small.

3. Reflectivity

To calculate the reflectivity we begin with the familiar expression (see, for example, Sears, 1978) for the double-differential cross section for coherent elastic scattering,

$$\frac{d^2\sigma}{d\Omega' d\varepsilon'} = |\langle b_{\mathbf{q}}\rangle|^2\,\delta(\omega). \tag{3.1}$$

Here $\mathbf{q}$ and ω are the momentum and energy transfers in units of $\hbar$,

$$\begin{aligned} \mathbf{q} &= \mathbf{k} - \mathbf{k}', \\ \omega &= \varepsilon - \varepsilon', \end{aligned} \tag{3.2}$$

where $\mathbf{k}$ and $\mathbf{k}'$ are the initial and final neutron wave vectors ($k = 2\pi/\lambda$) and $\varepsilon = \hbar k^2/2M$ in which M is the neutron mass. Also,

$$b_{\mathbf{q}} = \int b(\mathbf{r}) \exp(i\mathbf{q}.\mathbf{r})\,d\mathbf{r}, \tag{3.3}$$

where $b(\mathbf{r})$ is the microscopic scattering-length density,

$$b(\mathbf{r}) = \sum_j b_j\,\delta(\mathbf{r} - \mathbf{r}_j), \tag{3.4}$$

$\mathbf{r}_j$ and b_j being the position and bound coherent scattering length of the jth nucleus in the system. Finally, the brackets $\langle\rangle$ denote a thermodynamic average.

For a fixed value of $\mathbf{k}$,

$$d\mathbf{q} = d\mathbf{k}' = k'^2\, dk' d\Omega' = (Mk'/\hbar)\, d\varepsilon' d\Omega', \quad (3.5)$$

so that

$$\delta(\omega)\, d\Omega' d\varepsilon' = \frac{1}{k}\, \delta(\mathbf{k}.\mathbf{q} - \tfrac{1}{2}q^2)\, d\mathbf{q}. \quad (3.6)$$

Hence, the total cross section for coherent elastic scattering is given by

$$\sigma = \int d^2\sigma = \frac{1}{k} \int |\langle b_\mathbf{q}\rangle|^2\, \delta(\mathbf{k}.\mathbf{q} - \tfrac{1}{2}q^2)\, d\mathbf{q}. \quad (3.7)$$

Let us choose a system of Cartesian coordinate axes in which the z axis is normal to the face of the multilayer. If the multilayer is homogeneous in any xy plane then

$$\langle b(\mathbf{r})\rangle = f(z), \quad (3.8)$$

where

$$f(z) = \begin{cases} f_A = \rho_A b_A \text{ in the } A \text{ layers}, \\ f_B = \rho_B b_B \text{ in the } B \text{ layers}, \end{cases} \quad (3.9)$$

in which ρ_A and ρ_B are the corresponding atomic-number densities. Then

$$\langle b_\mathbf{q}\rangle = \int_0^{D_x} \int_0^{D_y} \int_0^{D_z} f(z) \exp[i(q_x x + q_y y + q_z z)]\, dx\, dy\, dz, \quad (3.10)$$

where D_x is the length of the multilayer in the x direction, *etc.* The quantity $\langle b_\mathbf{q}\rangle$ can then be expressed as a product of three factors.

$$\langle b_\mathbf{q}\rangle = XYZ, \quad (3.11)$$

where

$$X = [\exp(iq_x D_x) - 1]/iq_x, \quad (3.12)$$

with a similar expression for Y and

$$Z = \int_0^{D_z} f(z) \exp(iq_z z)\, dz. \quad (3.13)$$

The quantity $|X|^2$ can be expressed as

$$|X|^2 = 2\pi D_x\, \Delta(q_x), \quad (3.14)$$

where

$$\Delta(q_x) = \frac{D_x}{2\pi} \left[\frac{\sin(q_x D_x/2)}{q_x D_x/2}\right]^2, \quad (3.15)$$

and

$$\int_{-\infty}^{\infty} \Delta(q_x)\, dq_x = 1. \quad (3.16)$$

With a similar expression for $|Y|^2$ it then follows from (3.7) that

$$\sigma = \frac{4\pi^2 S}{k} \int_{-\infty}^{\infty} \int_{-\infty}^{\infty} \int_{-\infty}^{\infty} |Z|^2\, \Delta(q_x)\Delta(q_y)\delta(\mathbf{k}.\mathbf{q} - \tfrac{1}{2}q^2) \times dq_x\, dq_y\, dq_z, \quad (3.17)$$

where $S = D_x D_y$ is the area of the multilayer. In practice D_x and D_y are always large enough (>1 cm) that $\Delta(q_x)$ and $\Delta(q_y)$ are effectively δ functions. In this case the above integral can be evaluated immediately to give

$$\sigma = 8\pi^2 S|Z|^2/kq_z. \quad (3.18)$$

where

$$q_z = 2k \sin\theta. \quad (3.19)$$

Since the incident neutron current is $\Phi S \sin\theta$ and the reflected neutron current is $\Phi\sigma$ we see that the reflectivity is given by

$$R = \sigma/S \sin\theta. \quad (3.20)$$

Hence, it follows from (3.18) that

$$R = |A|^2, \quad (3.21)$$

where

$$A = \frac{4\pi}{q_z} \int_0^D f(z) \exp(iq_z z)\, dz, \quad (3.22)$$

and $D \equiv D_z$ is the thickness of the multilayer. The above expression for R is the same as is obtained from a Fresnel zone construction (Saxena & Schoenborn, 1977).

4. Ideal multilayer

For an ideal multilayer $f(z)$ is a periodic function with period d,

$$f(z + d) = f(z), \quad (4.1)$$

so that

$$A = (4\pi d/q_z)F(q_z)I(\alpha), \quad (4.2)$$

in which $F(q_z)$ is the unit bilayer structure factor,

$$F(q_z) = \frac{1}{d} \int_0^d f(z) \exp(iq_z z)\, dz, \quad (4.3)$$

and $I(\alpha)$ is the Laue interference function,

$$I(\alpha) = \sum_{l=1}^{N} \exp[2i(l-1)\alpha] = [1 - \exp(2iN\alpha)]/[1 - \exp(2i\alpha)]. \quad (4.4)$$

Here $N = D/d$ is the total number of bilayers and $\alpha = q_z d/2$.

We note first that

$$|I(\alpha)|^2 = \left(\frac{\sin N\alpha}{\sin \alpha}\right)^2, \tag{4.5}$$

and that this is a periodic function,

$$|I(\alpha + m\pi)|^2 = |I(\alpha)|^2, \tag{4.6}$$

where $m = 0, \pm 1, \pm 2, \ldots$. Hence, we can write, equivalently,

$$|I(\alpha)|^2 = \frac{2N\pi}{d} \sum_m \Delta(q_z - K_m), \tag{4.7}$$

where $K_m = 2m\pi/d$ represents the 'reciprocal-lattice vectors' and, since $N \gg 1$, $\Delta(q_z)$ reduces to the form (3.15). Since $\Delta(q_z - K_m)$ is appreciably different from zero only when $q_z \simeq K_m$ it follows that the reflectivity (3.21) becomes

$$R = \sum_m R_m, \tag{4.8}$$

in which

$$R_m = (32\pi^3 D/K_m^2)|F_m|^2 \Delta(q_z - K_m), \tag{4.9}$$

and

$$F_m = F(K_m) = \frac{1}{d}\int_0^d f(z) \exp(iK_m z)\, dz. \tag{4.10}$$

To facilitate the comparison of the present kinematical results with those of dynamical diffraction theory in § 6 it is convenient to express R_m in the equivalent form

$$R_m = \left(\frac{\sin xy}{x}\right)^2, \tag{4.11}$$

where

$$x = (q_z - K_m)\Delta_m/2\pi, \tag{4.12}$$

$$y = \pi D/\Delta_m, \tag{4.13}$$

and

$$\Delta_m = K_m/4|F_m| = m\pi/2d|F_m|. \tag{4.14}$$

In terms of the dimensionless variables x and y, R_m has its maximum value at $x = 0$ where

$$R_m(\max) = y^2. \tag{4.15}$$

Also, the integrated reflectivity is given by

$$\int R_m\, dx = \pi y, \tag{4.16}$$

so that the full width at half maximum (FWHM) of the Bragg peak, Δx, is given approximately by

$$\Delta x \simeq \pi/y. \tag{4.17}$$

Let us now define $k_m = 2\pi/\lambda_m$ such that

$$K_m = 2k_m \sin\theta, \tag{4.18}$$

in which case λ_m satisfies Bragg's law (2.1). Then, to first order,

$$q_z - K_m = (4\pi/\lambda_m^2)\sin\theta(\lambda_m - \lambda), \tag{4.19}$$

and

$$x = (\lambda_m - \lambda)/\Lambda_m, \tag{4.20}$$

where

$$\Lambda_m = \lambda_m^2/2\Delta_m \sin\theta = 4d^3 \sin\theta|F_m|/m^3\pi. \tag{4.21}$$

Hence, the maximum reflectivity is given by

$$R_m(\max) = (2Nd^2|F_m|/m)^2, \tag{4.22}$$

the integrated reflectivity (2.10) by

$$\beta_m = 8Nd^5 \sin\theta|F_m|^2/m^4, \tag{4.23}$$

and the FWHM of the Bragg peak is given approximately by

$$\Delta\lambda_m \simeq \lambda_m/mN. \tag{4.24}$$

The above results refer to an ideally collimated incident beam. In reality, the finite angular divergence of the incident beam will broaden the reflectivity curve so that $R_m(\max)$ will decrease and $\Delta\lambda_m$ will increase. However, in first approximation, the integrated reflectivity β_m, and hence the reflected flux (2.9), will be unaffected by the angular divergence of the incident beam.

5. Model bilayers

For the bilayer illustrated in Fig. 1,

$$f(z) = \begin{cases} f_A, & 0 < z < sd, \\ f_B, & sd < z < d, \end{cases} \tag{5.1}$$

s being the fractional thickness of the A layer. Then,

$$F_m = \begin{cases} f_A s + f_B(1-s), & m = 0, \\ (f_A - f_B)[\exp(2ms\pi i) - 1]/2m\pi i, & m \neq 0, \end{cases} \tag{5.2}$$

and, if $m \neq 0$,

$$|F_m|^2 = \left[(f_A - f_B)\frac{\sin(ms\pi)}{m\pi}\right]^2. \tag{5.3}$$

In particular, if the A and B layers are equally thick so that $s = 1/2$, then

$$|F_m|^2 = \begin{cases} [(f_A + f_B)/2]^2, & m = 0, \\ 0, & m = \pm 2, \pm 4, \ldots, \\ [(f_A - f_B)/m\pi]^2, & m = \pm 1, \pm 3, \ldots. \end{cases} \tag{5.4}$$

Here the even-order reflections are absent (Schoenborn *et al.*, 1974) and, for the odd-order reflections,

$$R_m(\max) = [2Nd^2(f_A - f_B)/m^2\pi]^2, \quad (5.5)$$

and

$$\beta_m = 8Nd^5 \sin\theta(f_A - f_B)^2/m^6\pi^2. \quad (5.6)$$

In practice the A and B material may interdiffuse so that the boundary between these two components will no longer be sharply defined. In the extreme case where the scattering-length density varies sinusoidally,

$$f(z) = \tfrac{1}{2}[(f_A + f_B) + (f_A - f_B)\sin(2\pi z/d)], \quad (5.7)$$

one finds that

$$F_m = \frac{1}{2}(f_A + f_B)\delta_{m,0} + \frac{i}{4}(f_A - f_B)(\delta_{m,1} - \delta_{m,-1}). \quad (5.8)$$

Hence,

$$|F_m|^2 = \begin{cases} [(f_A + f_B)/2]^2, & m = 0, \\ [(f_A - f_B)/4]^2, & m = \pm 1, \\ 0, & m = \pm 2, \pm 3, \ldots. \end{cases} \quad (5.9)$$

Relative to the previous results, the intensity of the first-order reflection is reduced by a factor $(\pi/4)^2 = 0{\cdot}617$ while all higher-order reflections are completely absent (Schoenborn *et al.*, 1974).

6. Extinction effects

The above results are all based on the expression (3.1) for the coherent elastic-scattering cross section which is obtained within the kinematical theory of neutron scattering, in which only single scattering is taken into account. These results are valid as long as $R_m(\max) \ll 1$ which requires that $y \ll 1$ and, hence, that $D \ll \Delta_m$. Multiple scattering and the associated extinction effects are taken into account in the dynamical theory of neutron diffraction (see, for example, Sears, 1978) which shows that

$$R_m = \frac{\sin^2[y(x^2-1)^{1/2}]}{x^2 - 1 + \sin^2[y(x^2-1)^{1/2}]}, \quad (6.1)$$

and, hence, that

$$R_m(\max) = \tanh^2 y, \quad (6.2)$$

and

$$\int R_m\, dx = \pi \tanh y. \quad (6.3)$$

When $y \ll 1$ these relations reduce to the corresponding kinematical results obtained in § 4.

For a symmetric bilayer ($s = 1/2$) the integrated reflectivity (2.10) now becomes

$$\beta_m = (\lambda_1/m^4 N_0)\tanh(N/m^2 N_0), \quad (6.4)$$

in which m is odd and

$$N_0 = \Delta_1/\pi d = \pi/2d^2|f_A - f_B|. \quad (6.5)$$

7. First-order reflected flux

The incident flux can be expressed as

$$\Phi(\lambda) = \Phi g(\lambda). \quad (7.1)$$

where

$$\int_0^\infty g(\lambda)\, d\lambda = 1, \quad (7.2)$$

so that $g(\lambda)\, d\lambda$ is the fraction of the incident flux in $d\lambda$. In particular, for an unfiltered thermal spectrum,

$$g(\lambda) = (2\lambda_0^4/\lambda^5)\exp[-(\lambda_0/\lambda)^2], \quad (7.3)$$

where

$$\lambda_0 = h(2Mk_BT)^{-1/2}. \quad (7.4)$$

Here h is Planck's constant, k_B Boltzmann's constant and T the temperature of the neutron source.

The first-order reflected flux is then given, according to (2.9), by

$$\Phi_1'/\Phi = \beta_1 g(\lambda_1) = \gamma(\lambda_0/\lambda_1)^4 \exp[-(\lambda_0/\lambda_1)^2], \quad (7.5)$$

where

$$\gamma = (2/N_0)\tanh(N/N_0). \quad (7.6)$$

Thus, the first-order reflected flux is given by the product of a wavelength-independent factor γ that depends only on the monochromator and a wavelength-dependent factor that depends only on the source.

Fig. 3 shows γ as a function of N for $N_0 = 100$. To obtain a large reflected flux it is desirable that $N \gtrsim N_0$. However, there is no advantage in having $N \gg N_0$. Thus, we may regard N_0 as the optimum value of N. The dashed line in Fig. 3 shows the kinematical result $\gamma = 2N/N_0^2$ which is valid when $N \ll N_0$.

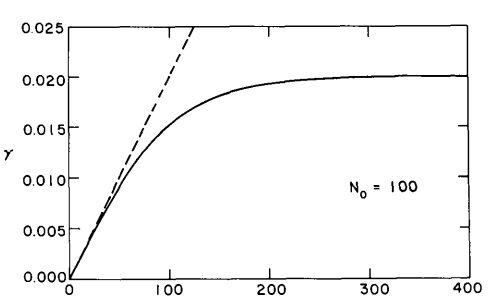

Fig. 3. The quantity γ as a function of the number of bilayers N. The solid curve is from the dynamical theory and the dashed line from the kinematical theory.

The quantity N_0 is shown in Fig. 4 for two commonly used bilayers Ge–Mn (Schoenborn *et al.*, 1974) and Ge–Fe (Lynn *et al.*, 1976). Since N_0 is proportional to d^{-2} the number of bilayers needed to saturate the reflected flux can be reduced by increasing the value of d. However, for a given wavelength $\lambda_1 = 2d \sin\theta$, the Bragg angle θ decreases as d increases so that, in practice, the minimum acceptable value of θ will place an upper limit on d.

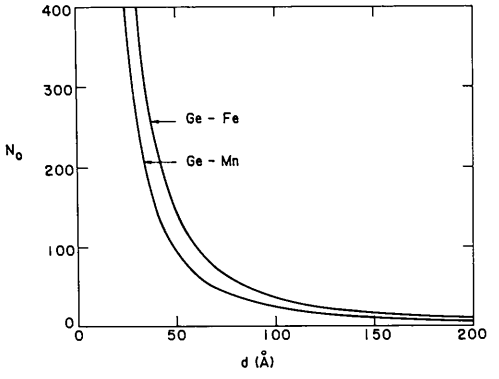

Fig. 4. The optimum number of bilayers N_0 as a function of the bilayer thickness d for two different bilayers.

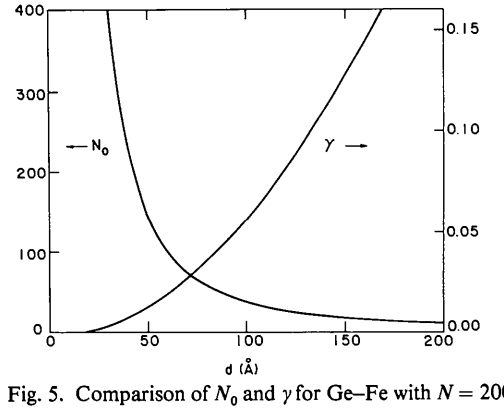

Fig. 5. Comparison of N_0 and γ for Ge–Fe with $N = 200$.

Another advantage in having d as large as possible is illustrated in Fig. 5 which compares the behavior of N_0 and γ as a function of d. It is seen that γ, and hence the first-order reflected flux, increases rapidly with increasing d.

Finally, the relative first-order reflected flux is shown in Fig. 6(*a*) as a function of λ_1 for a Ge–Fe multilayer with two different values of d. The source temperature is taken to be $T = 308$ K so that $\lambda_0 = 1{\cdot}76$ Å. The incident flux has its maximum at $(2/5)^{1/2}\lambda_0 = 1{\cdot}11$ Å while the reflected flux has its maximum at $2^{-1/2}\lambda_0 = 1{\cdot}24$ Å. Fig. 6(*a*) therefore describes the long-wavelength region where Φ_1' is approximately proportional to λ_1^{-4}.

8. Order contamination

The order contamination (2.13) is in general of the form

$$C_m = C_m^{\infty} \exp[-(m^2 - 1)(\lambda_0/\lambda_1)^2], \qquad (8.1)$$

where, for a symmetric bilayer ($s = 1/2$),

$$C_m^{\infty} = m \tanh(N/m^2 N_0)/\tanh(N/N_0) \qquad (8.2)$$

when m is odd and vanishes when m is even. Thus,

$$C_m^{\infty} = \begin{cases} 1/m, & N \ll N_0, \\ m, & N \gg N_0. \end{cases} \qquad (8.3)$$

The main contribution to the order contamination comes from C_3 which is shown as a function of λ_1 by the curve labeled $\delta/d = 0$ in Fig. 7. In practice, the order contamination may be smaller than is indicated here for two reasons. Firstly, any interdiffusion of the A and B components will tend to reduce the order contamination (Saxena & Schoenborn, 1977) as demonstrated in §5. Secondly, random variations in layer thicknesses will also reduce the order contamination. This effect is described by the curves with $\delta/d > 0$ in Fig. 7 and will be discussed in § 9. Of

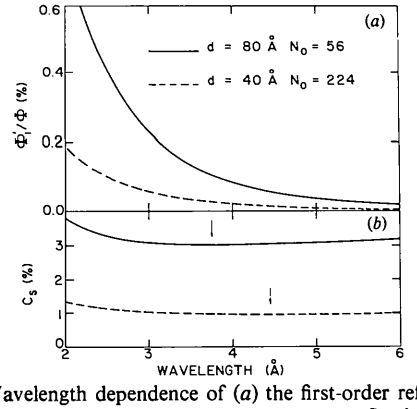

Fig. 6. Wavelength dependence of (*a*) the first-order reflected flux and (*b*) the contamination due to specular reflection for two different bilayer thicknesses of Ge–Fe.

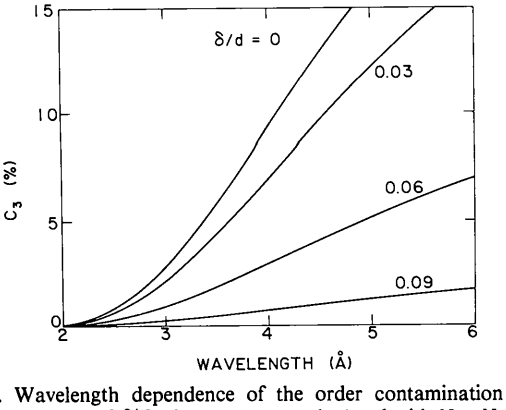

Fig. 7. Wavelength dependence of the order contamination for various values of δ/d. The curves are calculated with $N = N_0$ and $\lambda_0 = 1{\cdot}76$ Å.

course, the order contamination can, if necessary, be reduced still further by the use of crystalline filters or mechanical choppers in the usual way.

An alternative measure of the order contamination is given by the peak-height ratio in a θ–2θ scan,

$$\chi_m = R_m(\max)/R_1(\max) = [\tanh(N/m^2N_0)/\tanh(N/N_0)]^2. \quad (8.4)$$

Thus, for example, if $N = N_0$ we see that $\chi_3 = 2\%$ whereas $C_3^\infty = 44\%$. This demonstrates clearly that, even if the order contamination appears to be negligible in a θ–2θ scan (Schoenborn et al., 1974; Saxena & Schoenborn, 1975, 1977; Lynn *et al.*, 1976), it may still be appreciable when the multilayer is used as a monochromator.

9. Randomly modulated multilayer

We now discuss the effects that arise from the fact that the individual layers never have exactly the same thickness. We begin by considering an arbitrary multilayer for which

$$f(z) = \begin{cases} f_A, & z_l < z < z_l', \\ f_B, & z_l' < z < z_{l+1}, \end{cases} \quad (9.1)$$

where $l = 1, 2, \ldots, N$, and $z_1 = 0$ and $z_{N+1} = D$. Then (3.22) gives

$$A = \frac{4\pi}{iq_z^2}\sum_{l=1}^{N}\{f_A[\exp(iq_z z_l') - \exp(iq_z z_l)] + f_B[\exp(iq_z z_{l+1}] - \exp(iq_z z_l')]\}. \quad (9.2)$$

For an ideal multilayer,

$$z_l = (l-1)d, \qquad z_l' = (l-1/2)d, \quad (9.3)$$

and (9.2) reduces to (4.2) as it should.

In reality z_l and z_l' will at best have small random fluctuations about the average values

$$\langle z_l\rangle = (l-1)d, \qquad \langle z_l'\rangle = (l-1/2)d. \quad (9.4)$$

It then follows from the cumulant expansion

$$\langle\exp(iq_z z)\rangle = \exp[iq_z\langle z\rangle - \tfrac{1}{2}(q_z\Delta z)^2 + \ldots], \quad (9.5)$$

where Δz is the root-mean-square fluctuation in z,

$$(\Delta z)^2 = \langle(z - \langle z\rangle)^2\rangle = \langle z^2\rangle - \langle z\rangle^2, \quad (9.6)$$

that, in the Gaussian approximation,

$$\langle A\rangle = A^0\exp[-\tfrac{1}{2}(q_z\delta)^2], \quad (9.7)$$

where A^0 refers to the ideal multilayer and

$$\delta = \Delta z_l = \Delta z_l'. \quad (9.8)$$

Thus, the kinematical reflectivity becomes

$$R = R^0\exp[-(q_z\delta)^2], \quad (9.9)$$

so that, for the mth-order reflection,

$$R_m = R_m^0\exp(-2W_m), \quad (9.10)$$

where the exponential factor has been written in the form of a Debye–Waller factor with

$$2W_m = (K_m\delta)^2 = (2m\pi\delta/d)^2. \quad (9.11)$$

Similarly, the integrated reflectivity becomes

$$\beta_m = \beta_m^0\exp(-2W_m), \quad (9.12)$$

so that, finally, we obtain the following expression for the order contamination:

$$C_m = \frac{1}{m}\exp\left\{-(m^2-1)\left[\left(\frac{2\pi\delta}{d}\right)^2 + \left(\frac{\lambda_0}{\lambda_1}\right)^2\right]\right\}. \quad (9.13)$$

Fig. 7 shows C_3 as a function of λ_1 for various values of δ/d. We see that as δ/d increases the order contamination in the reflected beam decreases considerably.

When fluctuations in the layer thickness are taken into account (6.5) is replaced by

$$N_0 = (\pi/2d^2|f_A - f_B|)\exp[2(\pi\delta/d)^2]. \quad (9.14)$$

Thus, as δ increases, the value of N_0 also increases (Fig. 8) while the value of γ, and hence the first-order reflected flux, decreases.

10. Specular reflection

Specular reflection is also a multiple scattering phenomenon that is absent in the kinematical theory (see, for example, Sears, 1978, 1982). The specular reflectivity is given by

$$R_s = \left|\frac{1 - [1 - (\lambda/\lambda_c)^2]^{1/2}}{1 + [1 - (\lambda/\lambda_c)^2]^{1/2}}\right|^2, \quad (10.1)$$

where λ_c is the critical wavelength,

$$\lambda_c^2 = \pi\theta^2/F_0. \quad (10.2)$$

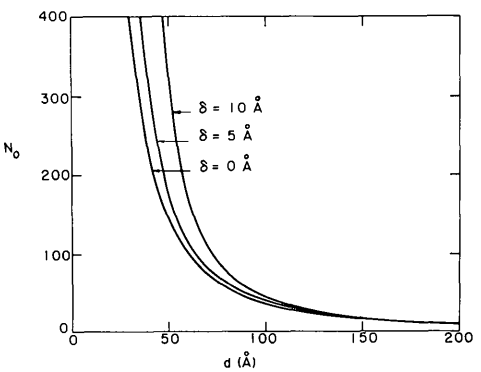

Fig. 8. Variation of N_0 with d for various values of δ. These curves refer to a Ge–Fe multilayer.

Since $F_0 = \frac{1}{2}(f_A + f_B)$ and $\theta \simeq \lambda_1/2d$ we see that

$$(\lambda_c/\lambda_1)^2 \simeq \pi/2d^2(f_A + f_B). \tag{10.3}$$

Thus, as illustrated earlier in Fig. 2,

$$R_s = \begin{cases} (1/16)[(\lambda/\lambda_c)^4 + (\lambda/\lambda_c)^6 + \ldots], & \lambda < \lambda_c, \\ 1, & \lambda > \lambda_c. \end{cases} \tag{10.4}$$

The general expression for the flux due to specular reflection is given by (2.8). In the usual situation where $\lambda_0 \ll \lambda_c$ this integral is given asymptotically by

$$\Phi'_s = (\Phi/8)(\lambda_0/\lambda_c)^4 \ln(\lambda_c/\lambda_0). \tag{10.5}$$

The contamination ratio C_s, which is defined by (2.12), is shown in Fig. 6(*b*) as a function of λ_1, for two different values of d. We see that C_s has a shallow minimum near $\lambda_1 = 4$ Å at the positions indicated by the arrows. It is evident that in practice the contamination of the reflected beam due to specular reflection will be typically 1 to 3%.

11. Polarization effects

Let us now consider a system such as Ge–Fe (Lynn *et al.*, 1976) in which the A layer is non-magnetic while the B layer is ferromagnetic. Then $f_A = \rho_A b_A$ as before but $f_B = \rho_B(b_B \pm b_M)$, where b_M is the effective magnetic scattering length and the plus (or minus) sign depends on whether the neutron spin is parallel (or antiparallel) to the atomic spins. Here

$$b_M = -\gamma r_e S F_M(\mathbf{q}), \tag{11.1}$$

where $\gamma = 1{\cdot}91$ is the neutron gyromagnetic ratio, $r_e = e^2/m_e c^2 = 2{\cdot}82$ fm is the classical electron radius and S is the average value of the atomic spin (*i.e.* $2S$ is the atomic magnetic moment in Bohr magnetons). Finally,

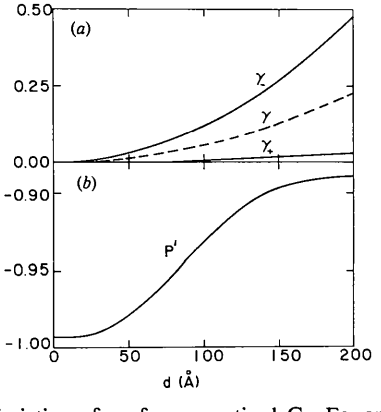

Fig. 9. (*a*) Variation of $\gamma_\pm$ for magnetized Ge–Fe, and of γ for unmagnetized Ge–Fe, as a function of d. (*b*) The corresponding polarization of the reflected neutron beam. The curves are calculated for $N = 200$.

$F_M(\mathbf{q})$ is the magnetic form factor. In the present application $\mathbf{q}$ is always small enough that we can put $F_M(\mathbf{q}) = F_M(0) = 1$.

Since the scattering length of the B layer depends on the neutron spin direction so does the reflectivity. Hence, the expression (7.5) for the first-order reflected flux becomes

$$\Phi'_\pm/\Phi_\pm = \gamma_\pm(\lambda_0/\lambda_1)^4 \exp[-(\lambda_0/\lambda_1)^2], \tag{11.2}$$

where

$$\gamma_\pm = (2/N_\pm)\tanh(N/N_\pm), \tag{11.3}$$

and

$$N_\pm = \pi/2d^2|\Delta f \mp f_M|, \tag{11.4}$$

in which

$$\Delta f = \rho_A b_A - \rho_B b_B, \quad f_M = \rho_B b_M. \tag{11.5}$$

The polarization of the incident beam is given by

$$P = (\Phi_+ - \Phi_-)/(\Phi_+ + \Phi_-), \tag{11.6}$$

with a similar expression for P', the polarization of the reflected beam. Hence,

$$P' = \frac{\gamma_+(1+P) - \gamma_-(1-P)}{\gamma_+(1+P) + \gamma_-(1-P)}. \tag{11.7}$$

In particular, if the incident beam is unpolarized ($P = 0$) then

$$P' = (\gamma_+ - \gamma_-)/(\gamma_+ + \gamma_-). \tag{11.8}$$

Fig. 9(*a*) shows $\gamma_\pm$ for magnetized Ge–Fe at room temperature together with the value of γ for the unmagnetized state. The corresponding polarization P' obtained from (11.8) is shown in Fig. 9(*b*). We see that polarizations >95% will be typical for this system. To obtain 100% polarization it would be necessary to match Δf and f_M exactly.

Discussions with B. M. Powell and P. Martel are gratefully acknowledged.

References

LYNN, J. W., KJEMS, J. K., PASSELL, L., SAXENA, A. M. & SCHOENBORN, B. P. (1976). *J. Appl. Cryst.* **9**, 454–459.

SAXENA, A. M. & SCHOENBORN, B. P. (1975). *Proceedings of the Symposium on Neutron Scattering for the Analysis of Biological Structures.* Brookhaven National Laboratory Report BNL 50453, pp. VII-30–VII-47.

SAXENA, A. M. & SCHOENBORN, B. P. (1977). *Acta Cryst.* **A33**, 805–813.

SCHOENBORN, B. P., CASPAR, D. L. D. & KAMMERER, O. F. (1974). *J. Appl. Cryst.* **7**, 508–510.

SEARS, V. F. (1978). *Can. J. Phys.* **56**, 1261–1288.

SEARS, V. F. (1982). *Phys. Rep.* **82**, 1–29.